

Geophysical Research Letters®

RESEARCH LETTER

10.1029/2023GL103005

Key Points:

- Cyclone Global Navigation Satellite System wind speeds and latent heat fluxes are used to study the diurnal cycle over the northern Australia coastal region
- Enhanced diurnal precipitation is associated with enhanced surface wind speed and convergence
- Diurnal precipitation and surface wind speed signals propagate westward in tandem from the Cape York Peninsula

Supporting Information:

Supporting Information may be found in the online version of this article.

Correspondence to:

H. X. Bui,
hien.bui@monash.edu

Citation:

Bui, H. X., Maloney, E. D., Short, E., & Riley Dellaripa, E. M. (2023). Diurnal cycle of wind speed and precipitation over the northern Australia coastal region: CYGNSS observations. *Geophysical Research Letters*, 50, e2023GL103005. <https://doi.org/10.1029/2023GL103005>

Received 24 JAN 2023

Accepted 7 APR 2023

Diurnal Cycle of Wind Speed and Precipitation Over the Northern Australia Coastal Region: CYGNSS Observations

Hien X. Bui¹ , Eric D. Maloney², Ewan Short³ , and Emily M. Riley Dellaripa² 

¹ARC Centre of Excellence for Climate Extremes, School of Earth, Atmosphere and Environment, Monash University, Clayton, VIC, Australia, ²Department of Atmospheric Science, Colorado State University, Fort Collins, CO, USA, ³School of Geography, Earth and Atmospheric Sciences, University of Melbourne, Parkville, VIC, Australia

Abstract The diurnal cycle of precipitation and its associated land-sea breeze circulation over coastal northern Australia are investigated using surface wind speed and enthalpy (latent and sensible heat) fluxes from the Cyclone Global Navigation Satellite System. Composite results during the austral summer of 2018–2022 show that diurnal precipitation propagates westward from the Cape York Peninsula into the Gulf of Carpentaria. The diurnal cycle of precipitation and surface wind speed are strongly coupled, with the wind speed maximum slightly leading the precipitation maximum. Additionally, analysis of the moist static energy budget shows that surface fluxes help support the westward-propagation of diurnal precipitation. These results—based on novel satellite data and reanalysis—are consistent with previous studies that have examined the impact of the land-sea breeze on the diurnal cycle of precipitation. The results provide a benchmark for model representation of this important atmosphere-ocean-land interaction.

Plain Language Summary The modulation of the diurnal cycle of precipitation over coastal northern Australia by surface winds was studied using the recently launched NASA Cyclone Global Navigation Satellite System (CYGNSS). Results show a strong connection between the daily cycles of precipitation and surface wind speed, with an offshore wind speed maximum leading the precipitation maximum by a few hours. Westward propagation of diurnal precipitation and wind speed signals occurs from the Cape York Peninsula into the Gulf of Carpentaria. A thermodynamic analysis supports the importance of the wind speed signal and associated surface fluxes for fostering offshore precipitation propagation. The novelty of this paper lies in the use of the new CYGNSS retrievals, which provide better space and time coverage of surface wind speed than previous satellite-based measurements and are not as negatively affected by precipitation contamination.

1. Introduction

The highest rainfall in Australia is observed in the northern region, where the climatological Southern Pacific Convergence Zone meets the coast of Queensland. Both onshore and offshore precipitation in this region is highly influenced by diurnal processes, with the amplitude of the precipitation diurnal harmonic approximately 50% the mean precipitation (Love et al., 2011). The diurnal precipitation cycle in coastal regions is associated with prominent land-sea breeze circulations, which are driven by the diurnally oscillating thermal contrast between land and adjacent ocean (e.g., Mapes et al., 2003a, 2003b; Yang & Slingo, 2001). These circulations can also affect other synoptic and mesoscale weather phenomena (Ichikawa & Yasunari, 2007; Mori et al., 2004), which in turn are linked to the larger-scale circulation through heating and divergence feedbacks (e.g., Schumacher et al., 2004). Documenting in detail the characteristics of the diurnal cycle of precipitation is thus important to understanding energy and water transports, large-scale circulations like monsoons and the Madden-Julian oscillation, and improving model simulations (e.g., Peatman et al., 2015).

The diurnal cycle of precipitation in the tropics is modulated by many climate modes, such as the Madden-Julian oscillation (MJO; Madden & Julian, 1971, 1972; Peatman et al., 2014) and the El Niño–Southern Oscillation (ENSO; Bain et al., 2010; Rauniyar & Walsh, 2013). Spatial-temporal variability of the tropical precipitation diurnal cycle is related to insolation, the land-sea breeze circulation, and topography, among many other processes (Gille et al., 2005; Lu et al., 2021; Natoli & Maloney, 2022; Yang & Smith, 2006). Early studies using satellite and in situ data found that tropical deep convection generally peaks over land in the late afternoon, and over the ocean in the early morning (e.g., Janowiak et al., 1994). Recently, Hassim et al. (2016) and Vincent and Lane (2016) found that the diurnal cycle of precipitation in the Maritime Continent propagates faster as it gets

© 2023. The Authors.

This is an open access article under the terms of the Creative Commons Attribution-NonCommercial-NoDerivs License, which permits use and distribution in any medium, provided the original work is properly cited, the use is non-commercial and no modifications or adaptations are made.

further from the coast, suggesting that propagation is primarily driven by density currents closer to the coast, but further offshore propagation is driven by gravity waves (Gille et al., 2005). Bai et al. (2021) also found similar behavior in and near Sumatra. Kilpatrick et al. (2017) reported that offshore surface wind convergence maxima lead the rainfall maxima by 1–2 hr in the western part of the Bay of Bengal and suggested that the land-sea breeze is a forcing mechanism for the diurnal precipitation cycle there. Short et al. (2019) examined the diurnal cycle of surface winds over the Maritime Continent and found that the relationship between precipitation and land-sea breeze circulations depends on coastline orientation and background flow.

The aforementioned studies have utilized a variety of data (e.g., global reanalysis, dropsondes/buoys, satellite scatterometry, and model simulations), and have tended to focus on the diurnal cycle of tropical precipitation and circulations (e.g., Alifdini & Shimada, 2022; Dai, 2023; Geng & Katsumata, 2023; Gille et al., 2005; Joseph et al., 2021; among many others). Less attention has been devoted to how surface wind speed and enthalpy flux variations may help modulate the tropical precipitation diurnal cycle in coastal regions. Previous modeling studies suggest that diurnally varying surface fluxes can be an important factor in modulating the diurnal cycle of tropical convection (Ruppert & Johnson, 2016). Additionally, previous studies of the diurnal cycle that relied on scatterometer-based measurements (e.g., Kilpatrick et al., 2017; Short et al., 2019; Turk et al., 2021) were limited to rain-free or light-rain regions as the microwave radar pulse from a scatterometer is attenuated in precipitation (e.g., Weissman et al., 2012).

In this paper, we first document the composite structure of precipitation, surface wind speed, and enthalpy (latent and sensible heat) fluxes associated with the diurnal cycle over the northern Australia coastal region during the austral summer (November–April) of 2018–2022. We use data from the recently launched National Aeronautics and Space Administration (NASA) Cyclone Global Navigation Satellite System (CYGNSS) that consists of a combination of eight microsatellites that estimate wind speed using measurements of direct global positioning system (GPS) signals and scattered GPS signals from the ocean surface (Ruf et al., 2016). The satellite constellation measurements have unprecedented temporal resolution and spatial coverage and are not significantly affected by precipitation. We then examine the mechanisms of the diurnal precipitation cycle in the context of the vertically-integrated moist static energy (MSE) budget highlighting the importance of surface fluxes and convergence for offshore diurnal precipitation propagation. Conclusions follow.

2. Data and Methodology

2.1. Data

We used the following data spanning November–April 2018–2022. All the data were regressed to a 0.5×0.5 latitude-longitude grid and 3-hourly temporal resolution prior to subsequent processing.

- *Cyclone Global Navigation Satellite System (CYGNSS)*: In this study, we analyze two recent CYGNSS wind speed products including the Science Data Record version 3.1 (SDR v3.1; CYGNSS, 2021b; Ruf et al., 2016) and Climate Data Record version 1.1 (CDR v1.1; CYGNSS, 2021a). Each product was generated from the full set of Level 2 wind speed data set following the algorithm suggested by Ruf (2018). The Level 2 wind speed products include the time-stamp and location of average wind speed at 25×25 km resolution from the Delay Doppler Mapping observations. The SDR v3.1 product incorporates real time monitoring of direct GPS signal strength and GPS satellite power fluctuations and thus produces more accurate wind speed retrievals than previous SDR versions. The CDR v1.1 is the latest climate-quality release of the CYGNSS wind speed product and uses a track-wise correction algorithm relative to reanalysis fields (Said et al., 2019) to remove biases due to fluctuations in the transmit power of GPS signals and other factors. As documented by Yi et al. (2019) and Li et al. (2021), CYGNSS can capture wind speed retrievals in coastal regions within 200 km away from the coastline; observations closer to the coast are sparser and more difficult to verify (see also Figure S1 in Supporting Information S1). Both of the CYGNSS wind speed products used here assume that the sea state is in equilibrium with the wind speed, or “fully developed seas,” which is the preferred product to use over most of the tropics away from tropical cyclones (Clarizia et al., 2018).

We also use the CYGNSS surface latent and sensible heat flux product SDR version 2.0 (SDR v2.0; CYGNSS, 2022c) that is based on the SDR v3.1 wind retrievals (e.g., Crespo et al., 2019).

- *Global Precipitation Measurement (GPM)*: We use precipitation from the Integrated Multi-satellitE Retrievals for GPM version 6 (Huffman et al., 2019) to diagnose diurnal precipitation variability, and to compare with

the CYGNSS-derived wind speed and fluxes. Given the availability of GPM data set, only data during austral summer of 2018–2021 are analyzed.

- *European Center for Medium-Range Weather Forecasts Reanalysis version 5 (ERA5)*: For comparison with the CYGNSS wind speed and GPM precipitation, we use 10 m winds from the ERA5 reanalysis (Hersbach et al., 2020). ERA5 data are also used to calculate terms in the vertically integrated MSE budget discussed below.

2.2. Methods

To examine the mechanisms regulating the diurnal cycle over northern Australia and in the offshore environment, we analyze the column integrated MSE (m) budget (e.g., Bui et al., 2016):

$$\left\langle \frac{\partial m}{\partial t} \right\rangle = - \left\langle \omega \frac{\partial m}{\partial p} \right\rangle - \langle \mathbf{v} \cdot \nabla m \rangle + \text{LH} + \text{SH} + \text{LW} + \text{SW}. \quad (1)$$

Here, p is the pressure, \mathbf{v} is the horizontal wind vector, and ω is the vertical pressure velocity. The brackets represent a mass-weighted integration through the troposphere from 1,000 to 100 hPa. In Equation 1 the MSE tendency, $\left\langle \frac{\partial m}{\partial t} \right\rangle$, is balanced by vertical MSE advection, $\left\langle \omega \frac{\partial m}{\partial p} \right\rangle$, horizontal advection, $-\langle \mathbf{v} \cdot \nabla m \rangle$, and the net fluxes into the atmospheric column that include surface latent heat flux (LH), surface sensible heat flux (SH), net longwave radiation (LW), and net shortwave radiation (SW). The net radiative fluxes are calculated as the difference between the surface and top of atmosphere fluxes. The vertical MSE advection represents the export or import of MSE by large-scale vertical motion and is associated with a quantity called gross moist stability that is used to characterize the impacts of convection on the MSE budget (Raymond et al., 2009). Each budget term is calculated from 3-hourly data. We note that the residual term is small, but not zero, possibly associated with the inconsistencies between the MSE advection and the diabatic MSE source, which is typically corrected in reanalysis products by an analysis increment.

The region of our analysis is northern Australia, including the coastal region (e.g., 10°S–30°S, 110°E–160°E). For most of our analysis, the daily mean was removed to highlight the diurnal cycle. Note that the Australian eastern standard time (AEST; UTC +11) and Australian western standard time (AWST; UTC +8) zones differ by 3 hr during the austral summer. Consequently, the time convention used here does not correspond to any specific local solar time.

3. Results

3.1. Composite Diurnal Cycle of Precipitation, Surface Wind Speed and Enthalpy Fluxes

We now examine the diurnal evolution of GPM precipitation and CYGNSS winds and enthalpy fluxes over the northern Australia coastal region. Readers are referred to the Supporting Information S1 for discussion about the climatological precipitation and wind speed over the northern Australia. To highlight the diurnal cycle signal, the daily mean was subtracted from the composite 3-hourly data (Figure 1). The precipitation shows strong differences between land and ocean and between morning and evening—about 09Z and 21Z (8 p.m. and 8 a.m. local time; Figures 1a–1d). A strong diurnal cycle also occurs over the Cape York Peninsula. In addition, the ERA5 10 m wind shows a front/dryline feature over inland Australia associated with strong wind convergence around 25°S and 120°E. This convergence is stronger in the early evening (e.g., Figure 1b), possibly due to a large change in moisture with a relatively small change in temperature (Arnup & Reeder, 2007). For reference, we show the results without removing the daily mean in Figure S3 in Supporting Information S1. The low-level westerly flow from western Australia converges with the easterly flow, reflecting the behavior of the Australian monsoon during austral summer. Although considerable spatial variability is present in Figure S3 in Supporting Information S1 as the daily mean was retained, the diurnal patterns are quite clear, especially over the Gulf of Carpentaria (discussed further below in Figure 2).

CYGNSS wind speed shows a pattern consistent with GPM precipitation, with stronger wind anomalies associated with positive precipitation anomalies over the Gulf of Carpentaria and near coastal regions of north Australia (Figures 1e–1h). We also note the consistency across the different generations of CYGNSS wind speed products, although the SDR v3.1 has a stronger signal than CDR v1.1 because some of the high wind speed values have been removed from CDR v1.1 associated with the track correction algorithm (Ruf & Twigg, 2020; see also Figure

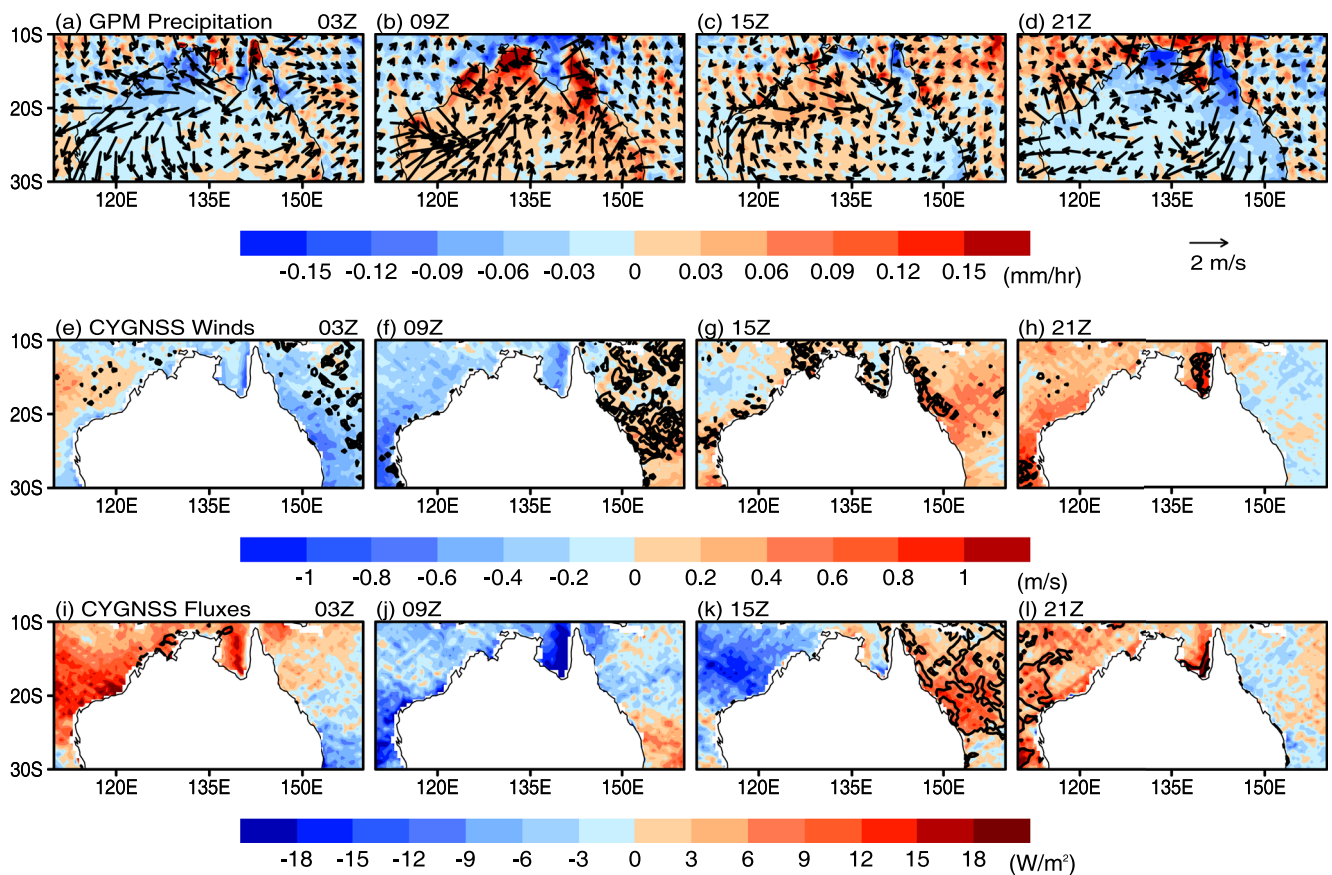


Figure 1. (a–d) Diurnal cycle of Global Precipitation Measurement precipitation (shaded, units are mm/hr) and ERA5 10 m wind vectors at (a) 03Z, (b) 09Z, (c) 15Z and (d) 21Z. (e–h) As in (a–d) but for CYGNSS wind speed SDR v3.1 (shaded, units are m/s) and CDR v1.1 (contours interval 0.2 m/s, only positive values are shown). See Figure S4 in Supporting Information S1 for differences between CYGNSS CDR v1.1 and SDR v3.1. (i–l) As in (a–d) but for CYGNSS latent heat flux (shaded, units are W/m^2) and sensible heat flux (contours interval 3 W/m^2 , only positive values are shown). Note that daily mean was removed to highlight the diurnal variation. See Figure S3 in Supporting Information S1 for the original data without removing daily mean.

S4 in Supporting Information S1). Latent heat flux anomalies show a similar pattern to the wind speed anomalies, although some differences exist over the west coast at 03Z where a coherent positive wind speed anomaly is not as apparent, suggesting a strong thermodynamic modulation to the flux signal. The positive sensible heat flux and latent heat flux anomalies often coincide, although the former is smaller in magnitude (Figures 1i–1l). To summarize, Figure 1 shows that there is a close correspondence between the diurnal cycle of precipitation and CYGNSS wind speed retrievals, such that increased wind speed can enhance the moisture supply to the column to support diurnal precipitation.

Figures 2a–2f show the difference between the evening (09Z or 8PM AEST) and the morning (21Z or 8AM AEST) GPM precipitation and CYGNSS products, including a focused region centered on the Gulf of Carpentaria. The diurnal cycle of precipitation over the Gulf of Carpentaria is among the strongest on the map, exceeding 0.2 mm/hr over a large area around 10.5°S–17.5°S (e.g., Figures 2a and 2d). Over this region, the precipitation differences are comparable to the mean precipitation (cf., Figure 2d and Figure S2a in Supporting Information S1), implying that diurnal rainfall produces a large fraction of the mean precipitation in this region. The ERA5 10 m wind shows the convergence of easterly and southwesterly diurnal wind anomalies inside the Gulf during periods of enhanced diurnal precipitation. There is also a strong land breeze directed from Cape York toward the Gulf, creating diverging wind anomalies over the Peninsula. Interestingly, over north-eastern Queensland, there are northerly wind anomalies, which may be associated with a diurnal enhancement of the monsoon trough as well as the land-breeze and mountain/valley-breeze coming from the Gulf of Papua (Short et al., 2019).

In contrast to the diurnal cycle of precipitation, the land-sea breeze signal in the CYGNSS wind speeds is strong only on the western shorelines of northern Australia; on the northeast side, the wind speed differences are small

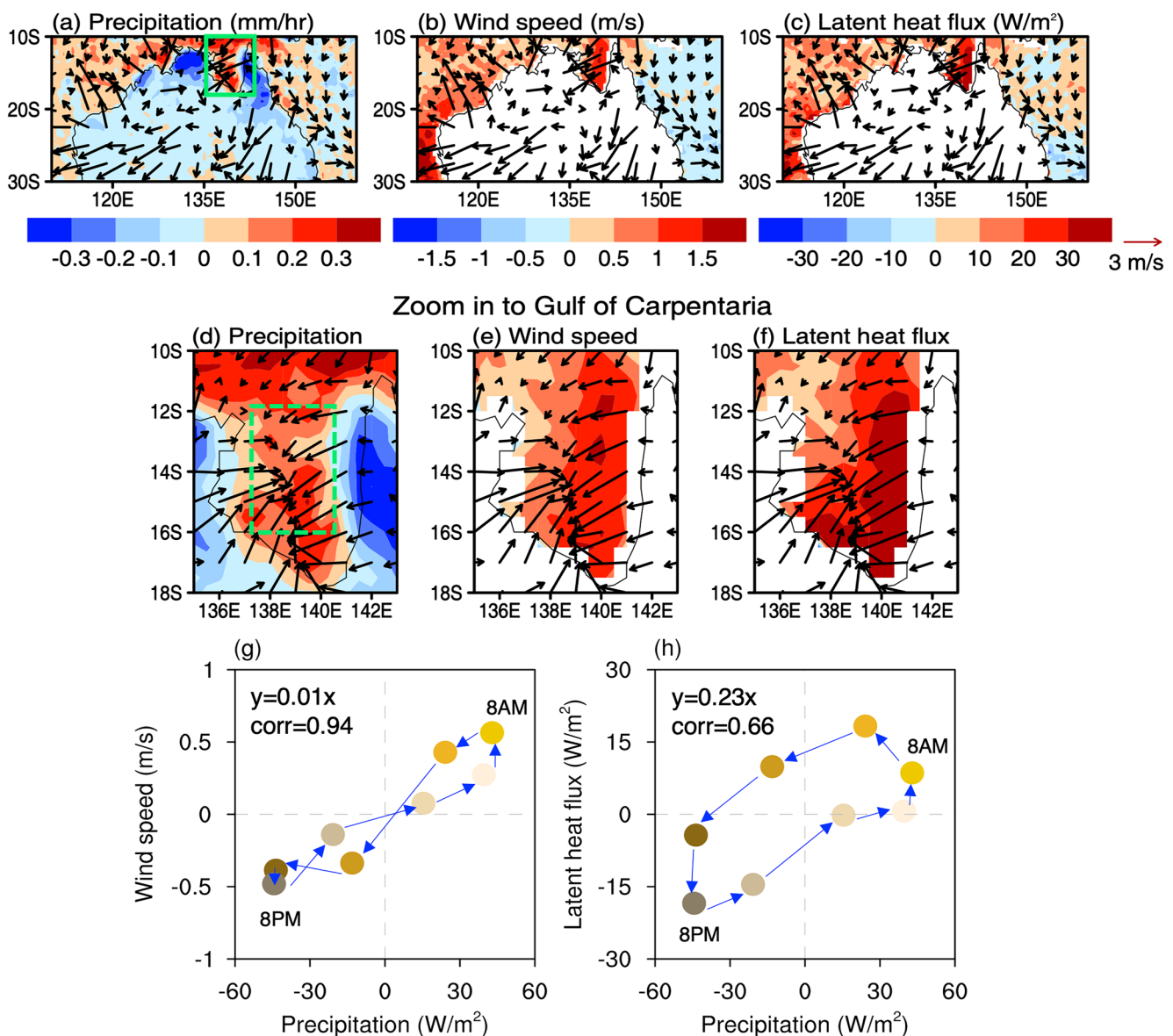


Figure 2. (a–c) Differences between 09Z and 21Z (8PM and 8AM AEST) for (a) Global Precipitation Measurement (GPM) precipitation (shaded, units are mm/hr), (b) CYGNSS wind speed SDR v3.1 (shaded, units are m/s) and (c) CYGNSS latent heat flux v2.0 (shaded, units are W/m²). Vectors are the ERA5 10 m winds. (d–f) Same as (a–d) but zoom in to Gulf of Carpentaria region (i.e., green box in a). (g–h) Scatterplot of GPM precipitation (x-axis, units are W/m²) and (g) CYGNSS wind speed (units are m/s) and (h) CYGNSS latent heat flux (units are W/m²) averaged over the Gulf of Carpentaria (12°S–16°S, 137°E–141°E; dashed green box in d). Dots represent 3-hourly data.

(Figure 2b). On the western side of the Cape York Peninsula, the difference in wind anomalies from one side of the Peninsula to the other may relate to the effect of the background winds. The strong easterly background winds may advect the coastal temperature gradient into the Gulf, so the maximum diurnal wind perturbations occur there. By contrast, on the eastern side, the temperature gradient is advected inland, so doesn't show up in the CYGNSS winds (Qian et al., 2009; Short et al., 2019). This reasoning aligns well with Natoli and Maloney (2022) and Fang and Du (2022) who showed that the strongest offshore-propagating diurnal variability occurs on the downwind sides of tropical landmasses. Analogous hypotheses for differences between the eastern and western sides of the Australian continent could be given, but the large difference in local solar times between these locations make it difficult to test such hypotheses with the present data. Regardless, CYGNSS reveals a strong diurnal variation in land/sea breeze circulations in the Gulf of Carpentaria with an amplitude exceeding 1.5 m/s (Figure 2e). The wind speed maximum shown here is consistent with Gille et al. (2003) who showed a strong sea

breeze near the coastal regions, and Brown et al. (2017) who studied the land-sea breeze off northern Australia using the Advanced Scatterometer (ASCAT). The results are also in agreement with Short et al. (2019) who noted the wind perturbations become even stronger during the Asian monsoon, and during inactive MJO phases, when the easterly background winds are stronger.

For the CYGNSS latent heat flux (Figures 2c and 2f), the positive flux anomalies show a similar pattern to the positive surface wind speed and precipitation anomalies. It is possible that a wind-induced surface heat exchange (WISHE) mechanism where enhanced surface wind speed increases latent heat flux that further enhances precipitation is important to the diurnal cycle of precipitation in this region as shown for other climate timescales (e.g., Araligidad & Maloney, 2008; Back & Bretherton, 2005; Bui et al., 2020), although more detailed examination is needed.

We also consider the phase relationship between GPM precipitation and CYGNSS products, averaged over the Gulf of Carpentaria (12°S – 16°S , 137°E – 141°E). Figure 2g shows that the diurnal CYGNSS wind speed and GPM precipitation perturbations are in phase suggesting that the land breeze forces/modulates the diurnal cycle of precipitation over this coastal region. On the other hand, the surface latent heat flux shows a lag of about 3 hr relative to precipitation and surface wind speed (Figure 2h), providing results contrary to the WISHE mechanism discussed above. However, surface fluxes still appear supportive of precipitation, and the precise timing of the precipitation and flux peaks are difficult to determine given the 3-hourly resolution of the datasets. The lagged response of the latent heat flux is an intriguing result, and it is possible that there is a strong thermodynamic component to the surface flux diurnal cycle with temperature of the sea surface also being important. Nevertheless, the correlation coefficient between wind speed and precipitation anomalies are 0.94, indicating that periods of enhanced diurnal precipitation are associated with enhanced surface wind speeds. Increased wind speed and associated fluxes can act with surface convergence to enhance the diurnal convection by increasing boundary layer moisture (e.g., Back & Bretherton, 2005; Ruppert & Johnson, 2015), as further examined below in term of moist static energy budget. The regression coefficient between the surface latent heat flux and precipitation indicates that latent heat flux anomalies are about 23% of the precipitation anomalies with a correlation of 0.66.

3.2. Westward Propagation of the Diurnal Cycle

Previous work has shown that the diurnal cycle of convection over the Cape York Peninsula and the Gulf of Carpentaria can be characterized by the initiation of sea-breeze forced convection in the mid-afternoon over the elevated topography of the Cape York Peninsula that matures during the evening and overnight as it moves westward toward the Gulf of Carpentaria and produces large-areal coverage of convectively-generated cirrus cloud (Keenan & Carbone, 2008). By the early morning, convection is maximized over the Gulf of Carpentaria aided by offshore flow from the outflows of land-based convection and amplified by the radiatively-driven mountain-to-valley breezes from the elevated terrain toward the coast (Keenan & Carbone, 2008).

To build on this previous work, we examine the relationship between the diurnal cycle of precipitation and the diurnal cycles of wind speed, latent heat flux, outgoing longwave radiation (OLR), and surface convergence using time-longitude Hovmöller diagrams averaged over the Gulf of Carpentaria (Figures 3a–3d). One notable feature in the precipitation and the environmental variables is the general westward propagation of the diurnal cycle. Maximum precipitation anomalies are generally accompanied by positive anomalies of surface wind speed (Figure 3a), latent heat flux (Figure 3b), convective activity (Figure 3c, denoted by the negative of OLR), and surface convergence (Figure 3d). The precipitation anomalies (contours) grow as they move westward off the Cape York coast and maximize between 138°E and 140°E at around 18–21Z (around 5–8AM AEST). Positive wind speed anomalies lead latent heat anomalies by a couple of hours (cf., Figures 3a and 3b), while slightly lagging the convergence maximum (cf., Figures 3a and 3d). Notably, the OLR anomalies are stronger near the coastline and weaken as they move further from the coast, and therefore smaller than the surface latent heat flux anomalies away from the coast (Figures 3b and 3c). Wind convergence (Figure 3d) develops from the coast and propagate to the center of the Gulf, consistent with previous studies done elsewhere in the tropics (e.g., Alifidini & Shimada, 2022; Dai & Deser, 1999; Geng & Katsumata, 2023). The low-level convergence and associated vertical motions foster diurnal precipitation over the tropical ocean (e.g., Dai, 2001). Overall, both CYGNSS wind speed and ERA5 winds indicate an increase in wind speed when the westward-propagating disturbances leave the coast at about 21Z (8PM AEST), possibly helping to support the diurnal convective features through flux anomalies and/or convergence.

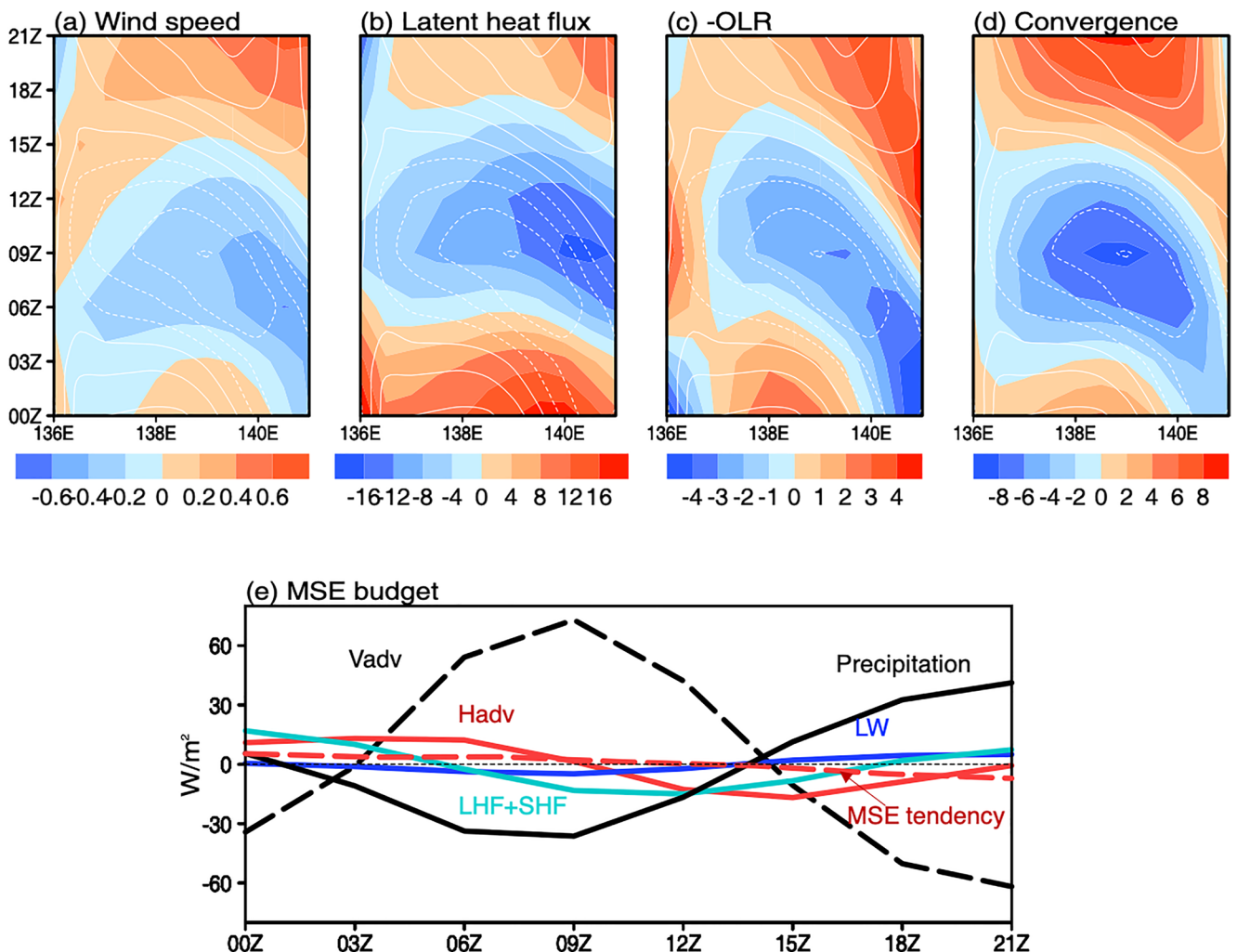


Figure 3. (a–d) Time-longitude plot of (a) CYGNSS wind speed SDR v3.1 (shaded, units are m/s), (b) CYGNSS latent heat flux (shaded, units are W/m²), (c) ERA5 outgoing longwave radiation (-OLR, shaded, units are W/m²), and (d) ERA5 surface convergence (shaded; scales are ×10⁶ s⁻¹). Contours in (a–d) are Global Precipitation Measurement (GPM) precipitation (units are W/m², contour interval ±12, dashed is negative and solid is positive). (e) Vertically integrated moist static energy (MSE) budget anomalies from the ERA5 and GPM precipitation anomalies (units are W/m²) averaged over the Gulf of Carpentaria (12°S–16°S, 137°E–141°E) as a function of time (hours). Terms include precipitation (black, solid), vertical advection (black, dashed), horizontal advection (red, solid), latent plus sensible heat fluxes (green, solid), longwave heating (blue, solid), and MSE tendency (red, dashed).

Given the strong westward-propagating signal of the diurnal cycle, we further examined the evolution of convection by examining each term of the MSE budget averaged across the Gulf of Carpentaria (Figure 3e). The MSE tendency term shows that the recharge of MSE occurs before the peak in precipitation (18Z–21Z or around 5–8AM AEST) with the discharge of MSE occurring during and after the precipitation peak. The vertical advection term is large and positive before peak precipitation and is negative during and after peak diurnal precipitation. The horizontal advection term is generally out of phase with the precipitation and of slightly smaller amplitude than that of vertical advection. The surface heat fluxes show a consistent result with Figures 2h and 3b that help to support precipitation. The dominance of the vertical advection term in the vertically integrated MSE budget suggests that shallow convection (accompanied by low-level convergence) is important for moistening the lower troposphere before the onset of deep convection.

To elaborate on the MSE results, we further investigate differences in MSE during days that have strong versus weak ambient winds, given the strong influences of prevailing direction and the speed of ambient winds on the diurnal cycle (e.g., Li et al., 2017; Qian et al., 2010). Since the eastern coastline of the Gulf of Carpentaria is straight, we define ambient winds as the daily mean easterly wind at 850 hPa (i.e., shore-orthogonal wind). Strong wind days are those in which the ambient wind speed is stronger than its mean plus one standard deviation of

the mean wind, while weak wind days are those with ambient wind weaker than the mean minus one standard deviation of the mean wind.

Figure 4 shows the diurnal evolution of the vertical structure of the MSE (shaded) and winds (vectors) anomalies during the strong and weak wind days. Under strong winds (Figures 4a–4e), the land breeze starts in the early evening (Figure 4a) and becomes stronger and deeper in the early morning (Figure 4b). The return flow aloft can also be seen clearly with a deep convection circulation (see also Figure S5 in Supporting Information S1). Notably, diurnal wind variations in the lower levels seem to decouple from those in the upper levels, and therefore there is only a weak land-sea breeze circulation, in agreement with Wei and Pu (2022). The MSE shows a tilted upward and outward structure from the western coast of the Cape York Peninsula, suggesting a downward phase propagation, consistent with the linear theory of internal gravity waves, which predicts that the divergence phase lines will be tilted from the horizontal direction (e.g., Kilpatrick et al., 2017; Rotunno, 1983). Low-level moistening appears near the coast of Cape York at 8PM AEST and fully develops and moves further westward at 8AM AEST (Figures 4a–4e), consistent with the westward propagation of diurnal precipitation (Figure 3). The dry/cold anomalies over the west side of the positive MSE anomalies during the strong wind days can contribute to the transition from shallow to deep convection and the propagation of precipitation (i.e., cold pool dynamics, see also Feng et al., 2015; Kharoutdinov & Randall, 2006; Wei & Pu, 2022). The dominance of the shallow convection mode can also increase the favorability of the atmosphere for deep convection and enhanced precipitation (e.g., Bui et al., 2019). The period of low-level moistening in Figure 4 is consistent with the vertical advection moistening signal in Figure 3e and the convergence signal in Figure 3d, and surface fluxes help to support the mature moisture anomaly as shown in Figure 3b. Under weak winds, the moistening process is weak (Figures 4f–4j), and the drying over the oceanic boundary layer occurs during 5AM–8AM AEST. The westward propagating diurnal cycle signal is also not clear during the weak wind days.

There are a few caveats to consider for the results derived here. The surface enthalpy fluxes are dependent on the fidelity of ERA5's surface thermodynamic fields and incur the attendant errors and biases. For comparison, we have shown some associated results using the ERA5 in Figures S6 and S7 in Supporting Information S1, which are qualitatively similar to the results using CYGNSS wind speed and fluxes. We also did not track the propagation of each individual convective system, and instead used the composites to visualize the evolution of the fields. Further, we did not study the interaction between the diurnal cycle of precipitation and MJO events or tropical cyclones, which are known to affect the diurnal cycle of precipitation (e.g., Peatman et al., 2014; Rauniyar & Walsh, 2011). There were no tropical cyclones during the time period of our study and there was only one strong MJO event (e.g., real-time multivariate MJO index is greater than 1, can be downloaded at <http://www.bom.gov.au/climate/mjo/>). Despite these caveats, the consistency between GPM precipitation, CYGNSS wind, and ERA5 MSE budget terms shown above give us confidence in the robustness of our conclusions about the co-propagation of precipitation and surface wind speed.

4. Concluding Remarks

CYGNSS retrievals during the austral summer (November–April) of 2018–2022 are used to study the diurnal cycle of surface wind speed over the Gulf of Carpentaria, where the amplitude of the diurnal cycle of precipitation is comparable to the mean precipitation. Although the basic dynamics of the diurnal cycle/land-sea breeze have been explored in several previous studies (e.g., Berry et al., 2011; Kilpatrick et al., 2017; Short et al., 2019, among others), satellite wind observations of diurnal convection-wind coupling, especially in satellite products that are not affected by rainfall, have not been utilized. Our results highlight the usefulness of the CYGNSS data set for investigating the diurnal cycle in this region and support previous findings on land-sea breeze coupling processes. In summary, the diurnal cycle composites show a coupling between the CYGNSS surface wind speed, surface fluxes, and GPM precipitation that indicates wind-induced fluxes may help to support diurnal disturbances as they propagate offshore (Figures 2 and 3). Physically, increased wind-induced surface fluxes and enhanced convergence destabilize the atmospheric column by increasing boundary layer moisture and MSE thus promoting or maintaining enhanced precipitation (e.g., Back & Bretherton, 2005; Ruppert & Johnson, 2015). In the Gulf of Carpentaria, the diurnal anomalies of both wind speed, fluxes, and precipitation propagate westward in tandem (Figures 3 and 4), consistent with the MSE budget. Westward propagation of diurnal convective disturbances in the Gulf of Carpentaria is supported by low-level convergence helping to moisten the offshore environment in advance of propagating diurnal precipitation, and wind-induced surface flux anomalies reinforcing moisture anomalies coincident with the precipitating region.

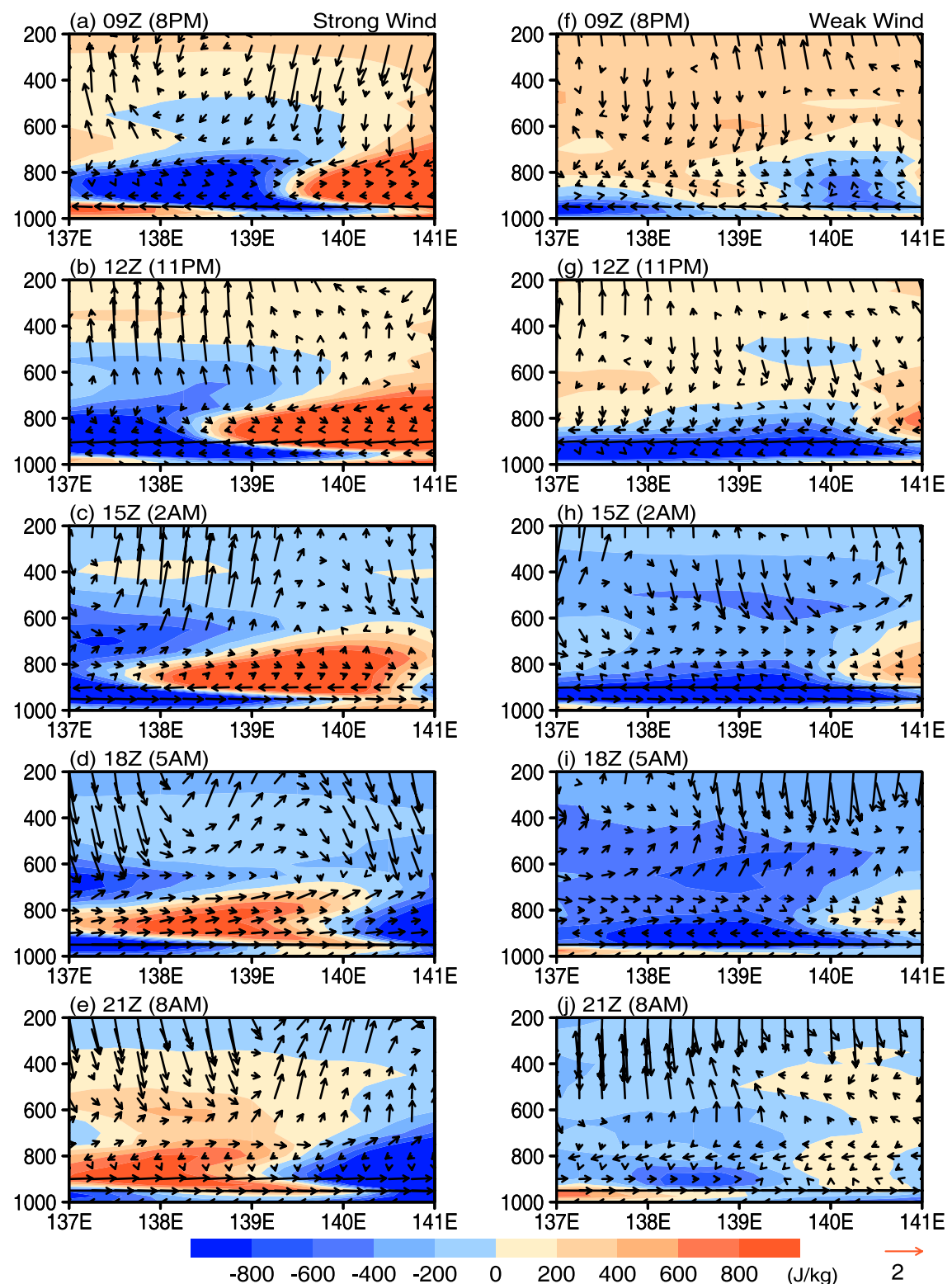


Figure 4. Pressure-longitude plot of ERA5 moist static energy (shaded, units are J/kg) and vertical circulation (i.e., shore-orthogonal wind and omega; vectors, units of horizontal wind are m/s and units of omega are 10^{-2} Pa/s) averaged over (a–e) strong and (f–j) weak wind days and over the Gulf of Carpentaria (12°S – 16°S). See Figure S5 in Supporting Information S1 for the omega.

With increased coverage and the ability to measure in regions of heavy rainfall, CYGNSS provides insights into diurnal processes that do not rely on the assumptions inherent in reanalysis data. Since the current results are based on 5 years of CYGNSS data, it is critical to re-examine the robustness of the results derived here as a longer CYGNSS data record becomes available, and as new versions of CYGNSS products with improved algorithms are developed. Regardless, a robust conclusion from our current study is that there is a coherent relationship between diurnal cycle of precipitation and surface wind speed. Further modeling work would be required to support its importance.

Data Availability Statement

CYGNSS wind speed and latent heat flux can be downloaded at <https://podaac.jpl.nasa.gov/CYGNSS>. The ERA5 data and GPM precipitation are obtained from <https://dx.doi.org/10.25914/5f48874388857> and <https://dx.doi.org/10.5067/GPM/IMERGDF/DAY/06>, respectively.

Acknowledgments

This study was supported by Australian Research Council under Grant CE170100023. EDM and ERD were supported by NASA CYGNSS Grant 80NSSC21K1004. We thank the NASA CYGNSS team for providing the wind speed and enthalpy fluxes products. Open access publishing facilitated by Monash University, as part of the Wiley - Monash University agreement via the Council of Australian University Librarians.

References

- Alifdini, I., & Shimada, T. (2022). Diurnal variation of surface wind divergence in the Maritime Continent using ASCAT and SeaWinds observations and ERA5 reanalysis data. *Sola*, 18(0), 154–158. <https://doi.org/10.2151/sola.2022-025>
- Araligidad, N. M., & Maloney, E. D. (2008). Wind-driven latent heat flux and the intraseasonal oscillation. *Geophysical Research Letters*, 35(4), L04815. <https://doi.org/10.1029/2007GL032746>
- Arnup, S. J., & Reeder, M. J. (2007). The diurnal and seasonal variation of the northern Australian dryline. *Monthly Weather Review*, 135(8), 2995–3008. <https://doi.org/10.1175/mwr3455.1>
- Back, L. E., & Bretherton, C. S. (2005). The relationship between wind speed and precipitation in the Pacific ITCZ. *Journal of Climate*, 18(20), 4317–4328. <https://doi.org/10.1175/JCLI3519.1>
- Bai, H., Deranadyan, G., Schumacher, C., Funk, A., Epifanio, C., Ali, A., et al. (2021). Formation of nocturnal offshore rainfall near the west coast of Sumatra: Land breeze or gravity wave? *Monthly Weather Review*, 149(3), 715–731. <https://doi.org/10.1175/mwr-d-20-0179.1>
- Bain, C. L., Magnusdottir, G., Smyth, P., & Stern, H. (2010). Diurnal cycle of the intertropical convergence zone in the east Pacific. *Journal of Geophysical Research: Atmosphere*, 115(D23), D23116. <https://doi.org/10.1029/2010JD014835>
- Berry, G., Reeder, M. J., & Jakob, C. (2011). Physical mechanisms regulating summertime rainfall over northwestern Australia. *Journal of Climate*, 24(14), 3705–3717. <https://doi.org/10.1175/2011jcli3943.1>
- Brown, A. L., Vincent, C. L., Lane, T. P., Short, E., & Nguyen, H. (2017). Scatterometer estimates of the tropical sea breeze circulation near Darwin with comparison to regional models. *Quarterly Journal of the Royal Meteorological Society*, 143(708), 2818–2831. <https://doi.org/10.1002/qj.3131>
- Bui, H. X., Maloney, E. D., Riley Dellaripa, E. M., & Singh, B. (2020). Wind speed, surface flux, and intraseasonal convection coupling from CYGNSS data. *Geophysical Research Letters*, 47(21), e2020GL090376. <https://doi.org/10.1029/2020GL090376>
- Bui, H. X., Yu, J., & Chou, C. (2016). Impacts of vertical structure of large-scale vertical motion in Tropical climate: Moist static energy framework. *Journal of the Atmospheric Sciences*, 73(11), 4427–4437. <https://doi.org/10.1175/jas-d-16-0031.1>
- Bui, H. X., Yu, J., & Chou, C. (2019). Impacts of model spatial resolution on the vertical structure of convection in the tropics. *Climate Dynamics*, 52(1–2), 15–27. <https://doi.org/10.1007/s00382-018-4125-3>
- Clarizia, M. P., Zavorotny, V., & Ruf, C. (2018). Level 2 wind speed retrieval. In *Algorithm theoretical basis document* (pp. 148–0138). CYGNSS Project Document. Rev 5.
- Crespo, J., Posselt, D., & Asharaf, S. (2019). CYGNSS surface heat flux product development. *Remote Sensing*, 11(19), 2294. <https://doi.org/10.3390/rs11192294>
- CYGNSS. (2021a). CYGNSS level 2 climate data record version 1.1. Ver. 1.1. [Dataset]. PO.DAAC. <https://doi.org/10.5067/CYGNSS-L2C11>
- CYGNSS. (2021b). CYGNSS level 2 science data record version 3.1. Ver. 3.1. [Dataset]. PO.DAAC. <https://doi.org/10.5067/CYGNSS-L2X31>
- CYGNSS. (2022c). CYGNSS level 2 ocean surface heat flux science data record version 2.0. Ver. 2.0. [Dataset]. PO.DAAC. <https://doi.org/10.5067/CYGNSS-L2H20>
- Dai, A. (2001). Global precipitation and thunderstorm frequencies. Part II: Diurnal variations. *Journal of Climate*, 14(6), 1112–1128. [https://doi.org/10.1175/1520-0442\(2001\)014<1112:GPATFP>2.0.CO;2](https://doi.org/10.1175/1520-0442(2001)014<1112:GPATFP>2.0.CO;2)
- Dai, A. (2023). The diurnal cycle from observations and ERA5 in surface pressure, temperature, humidity, and winds. *Climate Dynamics*. <https://doi.org/10.1007/s00382-023-06721-x>
- Dai, A., & Deser, C. (1999). Diurnal and semidiurnal variations in global surface wind and divergence fields. *Journal of Geophysical Research*, 104(D24), 31109–31125. <https://doi.org/10.1029/1999JD900927>
- Fang, J., & Du, Y. (2022). A global survey of diurnal offshore propagation of rainfall. *Nature Communications*, 13(1), 7437. <https://doi.org/10.1038/s41467-022-34842-0>
- Feng, Z., Hagos, S., Rowe, A. K., Burleyson, C. D., Martini, M. N., & de Szoeke, S. P. (2015). Mechanisms of convective cloud organization by cold pools over tropical warm ocean during the AMIE/DYNAMO field campaign. *Journal of Advances in Modeling Earth Systems*, 7(2), 357–381. <https://doi.org/10.1002/2014MS000384>
- Geng, B., & Katsumata, M. (2023). Daily and subdaily wind and divergence variations observed by a shipborne Doppler radar off the southwestern coast of Sumatra. *Journal of the Atmospheric Sciences*. (published online ahead of print 2023). <https://doi.org/10.1175/JAS-D-22-0170.1>
- Gille, S. T., Llewellyn Smith, S. G., & Lee, S. M. (2003). Measuring the sea breeze from QuikSCAT scatterometry. *Geophysical Research Letters*, 30(3), 1114. <https://doi.org/10.1029/2002GL016230>
- Gille, S. T., Llewellyn Smith, S. G., & Staton, N. M. (2005). Global observations of the land breeze. *Geophysical Research Letters*, 32(5), L05605. <https://doi.org/10.1029/2004GL022139>
- Hassim, M. E. E., Lane, T. P., & Grabowski, W. W. (2016). The diurnal cycle of rainfall over New Guinea in convection permitting WRF simulations. *Atmospheric Chemistry and Physics*, 16(1), 161–175. <https://doi.org/10.5194/acp-16-161-2016>

- Hersbach, H., Bell, B., Berrisford, P., Hirahara, S., Horányi, A., Muñoz-Sabater, J., et al. (2020). The ERA5 global reanalysis. *Quarterly Journal of the Royal Meteorological Society*, 146(730), 1–51. <https://doi.org/10.1002/qj.3803>
- Huffman, G. J., Stocker, E. F., Bolvin, D. T., Nelkin, E. J., & Tan, J. (2019). GPM IMERG final precipitation L3 1 day 0.1 degree x 0.1 degree V06. In A. Savchenko & M. D. Greenbelt (Eds.), *Goddard Earth sciences data and information services center (GES DISC)*. <https://doi.org/10.5067/GPM/IMERGDF/DAY/06>
- Ichikawa, H., & Yasunari, T. (2007). Propagating diurnal disturbances embedded in the Madden-Julian Oscillation. *Journal of Climate*, 34(18), L18811. <https://doi.org/10.1029/2007GL030480>
- Janowiak, J. E., Arkin, P., & Morrissey, M. (1994). An examination of the diurnal cycle in oceanic tropical rainfall using satellite and in situ data. *Monthly Weather Review*, 122(10), 2296–2311. [https://doi.org/10.1175/1520-0493\(1994\)122<2296:aeotdc>2.0.co;2](https://doi.org/10.1175/1520-0493(1994)122<2296:aeotdc>2.0.co;2)
- Joseph, J., Girishkumar, M. S., Varikoden, H., Thangaprakash, V. P., Shivaprasad, S., & Rama Rao, E. P. (2021). Observed sub-daily variability of latent and sensible heat fluxes in the Bay of Bengal during the summer. *Climate Dynamics*, 56(3–4), 917–934. <https://doi.org/10.1007/s00382-020-05512-y>
- Keenan, T. D., & Carbone, R. E. (2008). Propagation and diurnal evolution of warm season cloudiness in the Australian and Maritime Continent region. *Monthly Weather Review*, 136(3), 973–994. <https://doi.org/10.1175/2007mwr2152.1>
- Khairoutdinov, M., & Randall, D. (2006). High-resolution simulation of shallow-to-deep convection transition over land. *Journal of the Atmospheric Sciences*, 63(12), 3421–3436. <https://doi.org/10.1175/jas3810.1>
- Kilpatrick, T., Xie, S.-P., & Nasuno, T. (2017). Diurnal convection-wind coupling in the Bay of Bengal. *Journal of Geophysical Research: Atmospheres*, 122(18), 9705–9720. <https://doi.org/10.1002/2017JD027271>
- Li, X., Yang, D., Yang, J., Zheng, G., Han, G., Nan, Y., & Li, W. (2021). Analysis of coastal wind speed retrieval from CYGNSS mission using artificial neural network. *Remote Sensing of Environment*, 260, 112454. <https://doi.org/10.1016/j.rse.2021.112454>
- Li, Y., Jourdain, N. C., Taschetto, A. S., Gupta, A. S., Argüeso, D., Masson, S., & Cai, W. (2017). Resolution dependence of the simulated precipitation and diurnal cycle over the Maritime Continent. *Climate Dynamics*, 48(11–12), 4009–4028. <https://doi.org/10.1007/s00382-016-3317-y>
- Love, B. S., Matthews, A. J., & Lister, G. M. S. (2011). The diurnal cycle of precipitation over the Maritime Continent in a high-resolution atmospheric model. *Quarterly Journal of the Royal Meteorological Society*, 137(657), 934–947. <https://doi.org/10.1002/qj.809>
- Lu, J., Li, T., & Wang, L. (2021). Precipitation diurnal cycle over the Maritime Continent modulated by the climatological annual cycle. *Journal of Climate*, 34(4), 1387–1402. <https://doi.org/10.1175/jcli-d-20-0130.1>
- Madden, R. A., & Julian, P. R. (1971). Detection of a 40–50 day oscillation in the zonal wind in the tropical Pacific. *Journal of the Atmospheric Sciences*, 28(5), 702–708. [https://doi.org/10.1175/1520-0469\(1971\)028<702:DOADOI>2.0.CO;2](https://doi.org/10.1175/1520-0469(1971)028<702:DOADOI>2.0.CO;2)
- Madden, R. A., & Julian, P. R. (1972). Description of global-scale circulation cells in the Tropics with a 40–50 day period. *Journal of the Atmospheric Sciences*, 29(6), 1109–1123. [https://doi.org/10.1175/1520-0469\(1972\)029<1109:DGSCCC>2.0.CO;2](https://doi.org/10.1175/1520-0469(1972)029<1109:DGSCCC>2.0.CO;2)
- Mapes, B. E., Warner, T. T., & Xu, M. (2003b). Diurnal patterns of rainfall in northwestern South America. Part III: Diurnal gravity waves and nocturnal convection offshore. *Monthly Weather Review*, 131(5), 830–844. [https://doi.org/10.1175/1520-0493\(2003\)131<0830:dporin>2.0.co;2](https://doi.org/10.1175/1520-0493(2003)131<0830:dporin>2.0.co;2)
- Mapes, B. E., Warner, T. T., Xu, M., & Negri, A. J. (2003a). Diurnal patterns of rainfall in northwestern South America. Part I: Observations and context. *Monthly Weather Review*, 131(5), 799–812. [https://doi.org/10.1175/1520-0493\(2003\)131<0799:dporin>2.0.co;2](https://doi.org/10.1175/1520-0493(2003)131<0799:dporin>2.0.co;2)
- Mori, S., Jun-Ichi, H., Tauhid, Y. I., Yamanaka, M. D., Okamoto, N., Murata, F., et al. (2004). Diurnal land–sea rainfall peak migration over Sumatra Island, Indonesian Maritime Continent observed by TRMM satellite and intensive rawinsonde soundings. *Monthly Weather Review*, 132(8), 2021–2039. [https://doi.org/10.1175/1520-0493\(2004\)132<2021:dlrpmo>2.0.co;2](https://doi.org/10.1175/1520-0493(2004)132<2021:dlrpmo>2.0.co;2)
- Natoli, M. B., & Maloney, E. D. (2022). The tropical diurnal cycle under varying states of the monsoonal background wind. *Journal of the Atmospheric Sciences*. <https://doi.org/10.1175/jas-d-22-0045.1>
- Peatman, S. C., Matthews, A. J., & Stevens, D. P. (2014). Propagation of the Madden-Julian Oscillation through the Maritime Continent and scale interaction with the diurnal cycle of precipitation. *Quarterly Journal of the Royal Meteorological Society*, 140(680), 814–825. <https://doi.org/10.1002/qj.2161>
- Peatman, S. C., Matthews, A. J., & Stevens, D. P. (2015). Propagation of the Madden-Julian Oscillation and scale interaction with the diurnal cycle in a high-resolution GCM. *Climate Dynamics*, 45(9), 2901–2918. <https://doi.org/10.1007/s00382-015-2513-5>
- Qian, J., Robertson, A. W., & Moron, V. (2010). Interactions among ENSO, the monsoon, and diurnal cycle in rainfall variability over Java, Indonesia. *Journal of the Atmospheric Sciences*, 67(11), 3509–3524. <https://doi.org/10.1175/2010jas3348.1>
- Qian, T., Epifanio, C. C., & Zhang, F. (2009). Linear theory calculations for the sea breeze in a background wind: The equatorial case. *Journal of the Atmospheric Sciences*, 66(6), 1749–1763. <https://doi.org/10.1175/2008jas2851.1>
- Rauniyar, S. P., & Walsh, K. J. E. (2011). Scale interaction of the diurnal cycle of rainfall over the Maritime Continent and Australia: Influence of the MJO. *Journal of Climate*, 24(2), 325–348. <https://doi.org/10.1175/2010jcli3673.1>
- Rauniyar, S. P., & Walsh, K. J. E. (2013). Influence of ENSO on the diurnal cycle of rainfall over the Maritime Continent and Australia. *Journal of Climate*, 26(4), 1304–1321. <https://doi.org/10.1175/jcli-d-12-00124.1>
- Raymond, D. J., Sessions, S. L., Sobel, A. H., & Fuchs, Ž. (2009). The mechanics of gross moist stability. *Journal of Advances in Modeling Earth Systems*, 1(3), 9. <https://doi.org/10.3894/JAMES.2009.1.9>
- Rotunno, R. (1983). On the linear theory of the land and sea breeze. *Journal of the Atmospheric Sciences*, 40(8), 1999–2009. [https://doi.org/10.1175/1520-0469\(1983\)040<1999:otlot>2.0.co;2](https://doi.org/10.1175/1520-0469(1983)040<1999:otlot>2.0.co;2)
- Ruf, C. S. (2018). Algorithm theoretical basis document. Level 3 gridded wind speed. CYGNSS Project Document, 148–0319. Rev 1, 20 Aug. 2018.
- Ruf, C. S., Atlas, R., Chang, P. S., Clarizia, M. P., Garrison, J. L., Gleason, S., et al. (2016). New ocean winds satellite mission to probe hurricanes and tropical convection. *Bulletin of the American Meteorological Society*, 97(3), 385–395. <https://doi.org/10.1175/BAMS-D-14-00218.1>
- Ruf, C. S., & Twigg, D. (2020). Algorithm theoretical basis document. Level 1 & 2 trackwise corrected climate data record. CYGNSS Project Document. Rev 0, 26 Mar. 2020.
- Ruppert, J. H., Jr., & Johnson, R. H. (2015). Diurnally modulated cumulus moistening in the preonset stage of the Madden-Julian oscillation during DYNAMO. *Journal of the Atmospheric Sciences*, 72(4), 1622–1647. <https://doi.org/10.1175/JAS-D-14-0218.1>
- Ruppert, J. H., Jr., & Johnson, R. H. (2016). On the cumulus diurnal cycle over the tropical warm pool. *Journal of Advances in Modeling Earth Systems*, 8(2), 669–690. <https://doi.org/10.1175/2015MS000610>
- Said, F., Jelenak, Z., Park, J., Soisuvann, S., & Chang, P. S. (2019). A track-wise wind retrieval algorithm for the CYGNSS mission. In *JGARSS 2019–2020 IEEE international geoscience and remote sensing symposium* (pp. 8711–8714). <https://doi.org/10.1109/IGARSS.2019.8898099>
- Schumacher, C., Houze, R. A., Jr., & Kraucunas, I. (2004). The tropical dynamical response to latent heating estimates derived from the TRMM precipitation radar. *Journal of the Atmospheric Sciences*, 61(12), 1341–1358. [https://doi.org/10.1175/1520-0469\(2004\)061<1341:tdrlt>2.0.co;2](https://doi.org/10.1175/1520-0469(2004)061<1341:tdrlt>2.0.co;2)
- Short, E., Vincent, C. L., & Lane, T. P. (2019). Diurnal cycle of surface winds in the Maritime Continent observed through satellite scatterometry. *Monthly Weather Review*, 147(6), 2023–2044. <https://doi.org/10.1175/mwr-d-18-0433.1>

- Turk, F. J., Hristova-Veleva, S., & Giglio, D. (2021). Examination of the daily cycle wind vector modes of variability from the constellation of microwave scatterometers and radiometers. *Remote Sensing*, 13(1), 141. <https://doi.org/10.3390/rs13010141>
- Vincent, C. L., & Lane, T. P. (2016). Evolution of the diurnal precipitation cycle with the passage of a Madden–Julian oscillation event through the Maritime Continent. *Monthly Weather Review*, 144(5), 1983–2005. <https://doi.org/10.1175/MWR-D-15-0326.1>
- Wei, Y., & Pu, Z. (2022). Diurnal cycle of precipitation and near-surface atmospheric conditions over the maritime continent: Land–sea contrast and impacts of ambient winds in cloud-permitting simulations. *Climate Dynamics*, 58(9–10), 2421–2449. <https://doi.org/10.1007/s00382-021-06012-3>
- Weissman, D. E., Stiles, B. W., Hristova-Veleva, S. M., Long, D. G., Smith, D. K., Hilburn, K. A., & Jones, W. L. (2012). Challenges to satellite sensors of ocean winds: Addressing precipitation effects. *Journal of Atmospheric and Oceanic Technology*, 29(3), 356–374. <https://doi.org/10.1175/jtech-d-11-00054.1>
- Yang, G., & Slingo, J. (2001). The diurnal cycle in the Tropics. *Monthly Weather Review*, 129(4), 784–801. [https://doi.org/10.1175/1520-0493\(2001\)129<0784:tdcitt>2.0.co;2](https://doi.org/10.1175/1520-0493(2001)129<0784:tdcitt>2.0.co;2)
- Yang, S., & Smith, E. A. (2006). Mechanisms for diurnal variability of global tropical rainfall observed from TRMM. *Journal of Climate*, 19(20), 5190–5226. <https://doi.org/10.1175/jcli3883.1>
- Yi, Y., Johnson, J. T., & Wang, X. (2019). On the estimation of wind speed diurnal cycles using simulated measurements of CYGNSS and ASCAT. *IEEE Geoscience and Remote Sensing Letters*, 16(2), 168–172. <https://doi.org/10.1109/LGRS.2018.287235>

References From the Supporting Information

- Nicholls, N., Drosdowsky, W., & Lavery, B. (1997). Australian rainfall variability and change. *Weather*, 52(3), 66–72. <https://doi.org/10.1002/j.1477-8696.1997.tb06274.x>